https://doi.org/10.5194/essd-2019-97
Preprint. Discussion started: 17 June 2019

Open Access Earth System Science Data Discussions

# A distributed soil moisture, temperature and infiltrometer dataset for permeable pavements and green spaces

Axel Schaffitel[1], Tobias Schuetz[2], Markus Weiler[1]

[1]Faculty of Environment and Natural Resources, University of Freiburg, Freiburg i. Br., 79098, Germany
[2]Faculty of Regional and Environmental Sciences, University of Trier, Germany

*Correspondence to*: Axel Schaffitel (axel.schaffitel@posteo.de)

**Abstract.** Knowledge on water and energy fluxes is a key for urban planning and design. Nevertheless, hydrological data for urban environments is sparse and as a result, many processes are still poorly understood and thus inadequately represented within models. We contribute to reduce this shortcoming by providing a dataset, which includes time series of soil moisture and soil temperature measured underneath 18 different permeable pavements (PPs) and 4 urban greenspaces located within the city of Freiburg (Germany). Time series were recorded with a high temporal resolution of 10 min with a total of 65 individual soil moisture sensors and cover a measuring period of 2 entire years (Nov. 2016 – Oct. 2018). The recorded time series contain valuable information on the soil hydrological behavior and demonstrate the effect of surface properties and surrounding urban structures on soil temperatures. In addition, we performed double-ring infiltration experiments, which in combination with the soil moisture measurements yielded soil hydrological parameters for the PPs including porosity, field capacity and infiltration capacity. We present this unique dataset, which is a valuable source of information for studying urban water and energy cycles. We encourage its usage in various ways e.g. for model calibration and validation purposes, to study thermal regimes of cities and to derive urban water and energy fluxes. The dataset is freely available at the FreiDok plus data repository at https://freidok.uni-freiburg.de/data/149321 and https://doi.org/10.6094/UNIFR/149321 (Schaffitel et al., 2019).

## 1 Introduction

Knowledge of urban water and energy fluxes is a key for urban planning and design. Although, there are various urban hydrological (see Elliott and Trowsdale, 2007 for a review on urban hydrological and drainage models) and energy balance models (see Grimmond et al., 2010 for an overview), there is only limited data available for validating and calibrating these models (Litvak et al., 2017; Salvadore et al., 2015; Schirmer et al., 2013). As a result, many processes remain unclear and are poorly represented within models (Salvadore et al., 2015). To overcome this shortcoming, Vereecken et al. (2015) emphasize the possibilities of new measurement technologies.

Urbanization leads to profound changes of water and energy cycles (Oke, 1988; Shuster et al., 2005). Impacts of alternated energy fluxes include the formation urban heat islands (UHIs) in the atmosphere, but also in the subsurface of cities (Oke et al., 2017). Impacts on the water balance include increased surface runoff volumes (Fletcher et al., 2013; Shuster et al., 2005) at the expense of soil infiltration (Cristiano et al., 2017; Salvadore et al., 2015; Schirmer et al., 2013) and evapotranspiration (Fletcher et al., 2013; Grimmond and Oke, 1991). One possibility to mitigate the hydrological impacts of urbanization is to replace impermeable surface covers with permeable pavements (PPs). Although, their usage is restricted mainly to parking spaces, pedestrian roads and roads with low traffic volumes, PPs can cover great parts of cities (Winston et al., 2016). Positive effects include the reduction of surface runoff volumes, reduction in peak flows as well as increases in evaporation and groundwater recharge rates (Andersen et al., 1999; Fassman and Blackbourn, 2010; Park et al., 2014; Scholz and Grabowiecki, 2007; Timm et al., 2018).

Soil moisture ($\theta$) is of major importance for understanding water and energy fluxes in terrestrial systems (Eagleson, 1978; Lahoz and De Lannoy, 2014; Trenberth and Asrar, 2014). One example is the partitioning of rainfall into surface runoff and infiltration which depends decisively on the state of the soil storage (Brocca et al., 2008). Although, this partitioning is of special interest for urban stormwater management, the effect of $\theta$ on the hydrologic performance of PPs is still under debate and different results exist in literature. While some authors reported antecedent moisture conditions to effect the hydrologic performance of PPs (Brown and Borst, 2015; Fassman and Blackbourn, 2010), other authors only found limited effect of antecedent moisture conditions (Guo et al., 2018). We anticipate that this debate will benefit from continuous $\theta$-measurements below PPs. So far, such measurements were used to analyze the applicability of time-domain reflectometry in coarse structured soils (Ekblad and Isacsson, 2007; Stander et al., 2013), to derive water fluxes (Ragab et al., 2003), for calibration of plot scale soil hydrologic models (Kodešová et al., 2014; Turco et al., 2017) and to study clogging dynamics of PPs (Razzaghmanesh and Borst, 2018). As far as known to the authors, a comprehensive analysis of $\theta$-dynamics beneath PPs did not take place so far. In contrast to $\theta$-measurements, infiltration experiments have been performed by various authors.

https://doi.org/10.5194/essd-2019-97
Preprint. Discussion started: 17 June 2019

They were used e.g. to derive the infiltration capacity of PPs (Illgen, 2009), study clogging dynamics (Borgwardt, 2006; Lucke and Beecham, 2011) and analyze the effect of road maintenance on infiltration rates (Winston et al., 2016).

Soil temperature ($T_{soil}$) contains important information on surface and subsurface thermal regimes. Their study is of importance, as subsurface temperatures effect the groundwater quality and the gas exchange of soils (Oke et al., 2017), but also have implications for the use of geothermal energy (Zhu et al., 2010). Furthermore, $T_{soil}$ can be used to derive the ground heat flux (GHF) (Kimball et al., 1976). Thereby, the GHF of urban areas is of special interest, as it is the main driver for the formation of subsurface UHIs (Menberg et al., 2013) and fundamental for closing the urban energy balance (Grimmond and Oke, 1991; Roberts et al., 2006). Nevertheless, values for the urban GHF are sparse and calculations often depend on parameter assumptions leading to high uncertainties. We are convinced that $T_{soil}$–observations will improve the prediction of the urban energy balance and reveal new findings on the formation and magnitude of subsurface UHIs.

According to Salvadore et al. (2015), there is a special need for measurements within urban soils. As far as we know, there is neither $\theta$ nor $T_{soil}$ data freely available for urban environments. Here we provide a unique dataset comprising of $\theta$ and $T_{soil}$ measured below PPs and green spaces located within an urban environment. Furthermore, we performed infiltration experiments which together with the $\theta$-time series were used to derive soil hydrological parameters for PPs. As porous surface covers (porous asphalt, porous concrete and porous paving stones) play a minor role within the study area, they are not part of dataset. Instead, data for PPs is limited to surface covers consisting of impermeable pavers separated by permeable joints (e.g. interlocking concrete pavers, cobblestones, grass pavers). We are convinced that the provided dataset is of great value for studying urban water and energy fluxes and encourage its usage within the fields of urban hydrology and urban climatology.

## 2. Study area

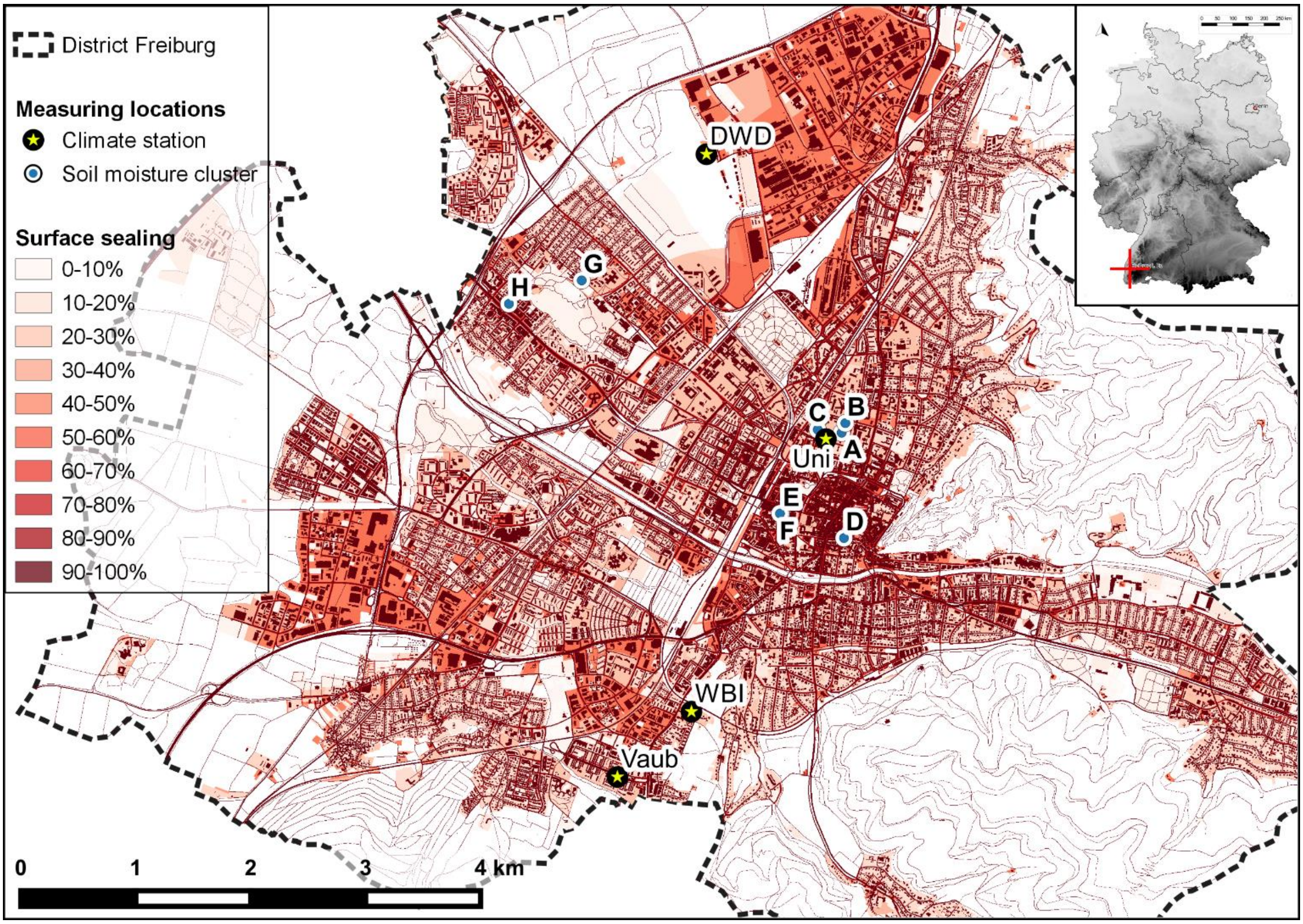

**Figure 1: Location of the soil moisture clusters and the climate stations within the city of Freiburg. Colors indicate the degree of surface sealing** (LUBW, 2012)**. Geodata of Germany in the upper right box originates from the Federal Agency for Cartography and Geodesy of Germany, while geodata of Freiburg was provided by the city of Freiburg.**

Soil moisture measurements were carried out in the city of Freiburg i. Br., which lies in the southwest of Germany (Figure 1). Natural soils found within the district of Freiburg are dominated by Cambisols and Luvisols at surrounding hillsides, whereas Fluvisols and Gleysols prevail within the valleys (soil map 1:50.000 federal state authority for Geology and Natural Resources of Baden-Württemberg). Urbanization impacts natural soils and strongly alters their properties (Wessolek, 2008). Therefore large parts of natural soils within cities were transformed into Technosols and Anthrosols (Kodešová et al., 2014). The study area is located in a temperate climate with a mean annual precipitation (*P*) of 894 mm and an annual mean air temperature of 11.5°C (evaluated for the period 1996-2015 for the climate station of the German Weather Service (DWD)). Rainfall is seasonally uneven distributed with more rainfall occurring during summer due to convective storms. The two hydrological years studied (Nov. 2016 – Oct. 2018) were characterized by around 200 mm/year less P compared to the long-term average (Figure 2).

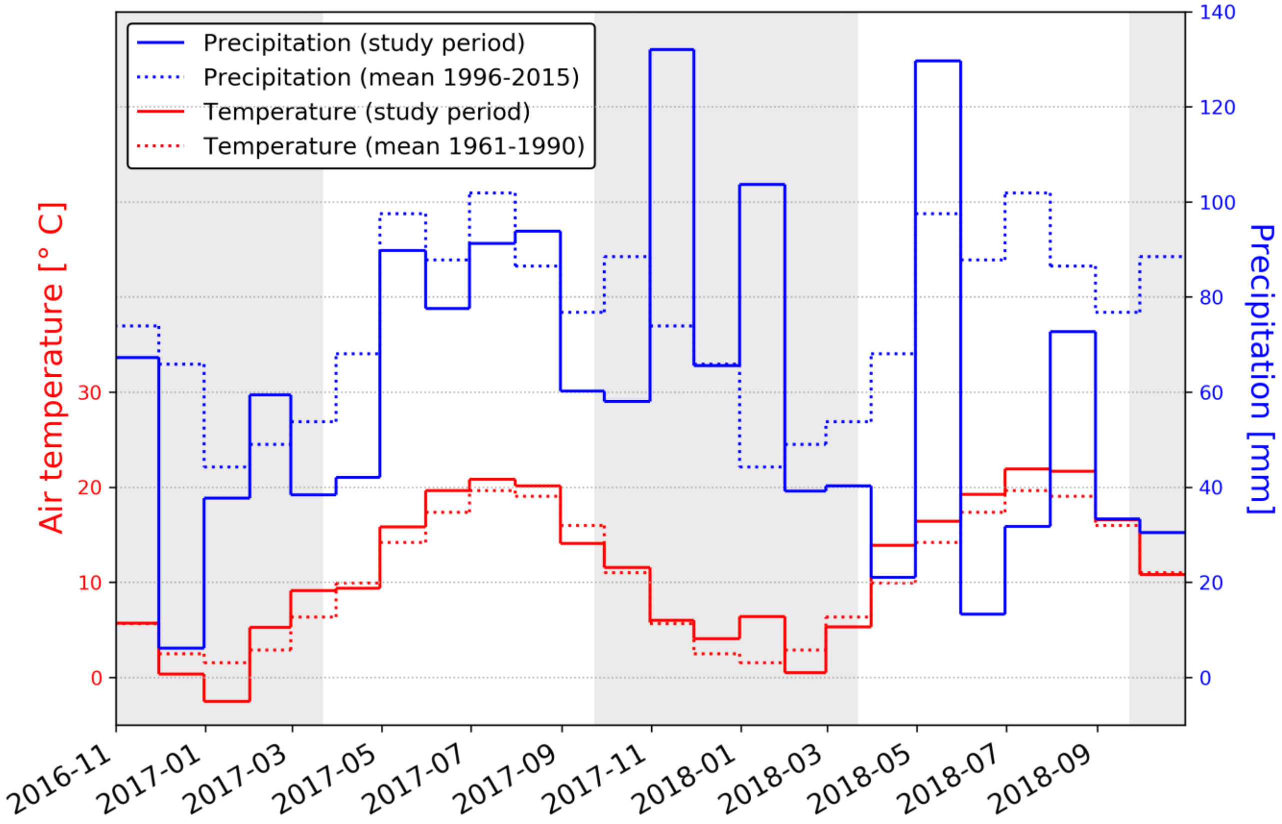

5 **Figure 2: Monthly precipitation sum and mean air temperature recoded at the climate station DWD within the study period compared to long-term mean values. The light grey background indicates the winter half year.**

## 3. Material and methods

### 3.1 Permeable pavements

According to German regulations, PPs must be designed to fully infiltrate a 10-minute lasting rainfall with a return period of 5 years. To ensure this, the surface must show an infiltration capacity of at least 97.2 mm/h (Borgwardt, 2001). Furthermore, the saturated hydraulic conductivity of underlying soils should exceed 19.4 mm/h. In case of lower permeability, the installation of underdrains is required. Figure 3 shows the typical layers of a permeable pavement which is built in accordance to national regulations (Borgwardt, 2001; FGSV, 2012). Thereby, the structure may be adapted locally, depending e.g. on constructional requirements and on the permeability of underlying soils. Paving stones, bedding, base and subbase layers consist of technical substrates which are installed during construction works. Their main function is to absorb and distribute pressures equally and to drain infiltrating water rapidly and thus to ensure the bearing capacity and the frost-resistance of the pavement layer. In most cases, the subbase layer lies directly above heavily compacted natural soils. Only in special cases, a subgrade is needed below the subbase layer (Borgwardt, 2001). PPs and their underlying layers belong to the soil class of Technosols.

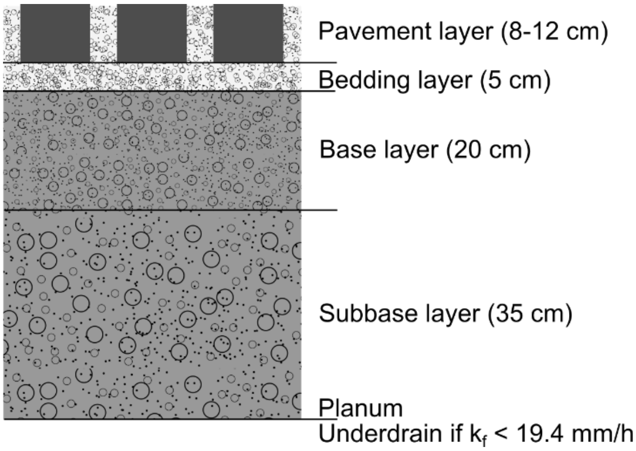

**Figure 3: Layers of a typical permeable pavement build in accordance to national regulations.**

https://doi.org/10.5194/essd-2019-97
Preprint. Discussion started: 17 June 2019

### 3.2 Climate data

Climate data for the study region was measured at the stations depicted in Figure 1 (see chapter data availability for URLs). The State Viniculture Institute Freiburg operates the WBI climate station and data with a temporal resolution of 10 min was provided upon request by the Center for Agricultural Technology Augustenberg (belonging to the Ministry of the Environment, Rural Affairs and Consumer Protection of the state Baden-Württemberg). For the study period, time series recorded at the stations DWD and WBI are free from data gaps. The DWD station operates according to guidelines of the world meteorological organization and therefore, is unbiased by urban effects. In contrast, the other three remaining stations are affected by the urban climate, as they are located in the vicinity of urban structures. The climatic input of the soil moisture measurements is assumed to be best represented by the WBI station, as it is the only urban climate station that is free from data gaps. For event separation, rain events were defined as rainy periods exceeding a minimum of 0.5 mm and separation took place when no rainfall was recorded for at least 2 h. In order to account for the spatial variability of urban rainfall (Cristiano et al., 2017) the event separation was based on the $P$ data recorded at both gap-free climate stations (DWD and WBI). In this way, a total of 302 individual events were separated for the study period (Nov. 2016 until Oct. 2018). Daily sum of reference crop evapotranspiration ($et_0$) was calculated for the WBI climate station by using the Pennman-Monteith equation and the parametrization recommended by Allen et al. (1998).

### 3.3 Measurement network

The soil measurement locations (hereinafter called plots) are organized in clusters with each cluster comprising several different surfaces (see Figure 1 for the location of the clusters). All studied PPs are located on either parking lots, pedestrian roads or residential roads with low traffic volumes. On each plot, infiltration experiments were performed and soil moisture sensors (SMT100, Truebner GmbH, Mannheim, Germany) were installed in 2-4 depths below the ground surface. Installation of the SMT100 sensors took place during two field campaigns in March and June 2016. For the installation, the existing pavement was removed and sensors were inserted into the undisturbed profile wall under undisturbed pavements. In order to avoid water ponding on the sensors and to minimize the disturbance of vertical vapor fluxes, they were installed horizontally with the narrow side in vertical direction. Afterwards, the plots were refilled with the original base and bedding material. Finally, municipal construction workers restored the paving layer professionally. Installation of the SMT100 sensors was often challenging due to the high compaction of soils and the presence of coarse aggregates. Therefore, we decided for some plots to insert sensors not into the profile wall but instead install them within the excavated hole which then was refilled successively with bedding material. Each cluster was equipped with an individual data logger accommodated in a small manhole. Variables measured by the SMT100 include the apparent dielectric permittivity ($\varepsilon_a$) and the soil temperature ($T_{soil}$) and were recorded by the data logger with a time interval of 10 min. Figure 4 shows the

https://doi.org/10.5194/essd-2019-97
Preprint. Discussion started: 17 June 2019

installation of the soil moisture sensors at the plots of cluster D as well as the small manhole used for accommodating the logger.

Figure 4: Installation of the soil moisture sensors at the plots of cluster D and the small manhole used for accommodating the data logger.

During the installation, soil samples were taken and the characteristics of the joints were analyzed. Recorded joint characteristics include joint material, joint condition, mean joint depth and joint vegetal cover. The mean joint depth was calculated from 10 individual measurements performed with a high precession slide gauge with a resolution of 0.1 mm. Joint conditions were classified into 4 categories ranging from 0 (very good condition) to 3 (very bad condition). This was achieved by a combination of visual categorization and finger testing of the joint material (not performed at PPs with mortar filled joints). Thereby, higher amount of fines were attributed to higher clogging and consequently to worse joint condition. Similarly, joint vegetal cover (consisting of tread-resistant plant communities and mosses) was classified visually into 4 categories ranging from 0 (no vegetation) to 3 (fully covered by vegetation). Finally, image analysis tools were used to determine the proportion of joints and the sealing degree. For this purpose, a 1 m x 1 m frame was mounted on the surfaces and pictures were taken. The images were fist corrected for geometric distortion by using an adapted version of the algorithm described in Weiler and Flühler (2004). Afterwards paving stones were digitized manually and their areal proportion was calculated. Table 1 shows the plots of the measurement network and their characteristics.

https://doi.org/10.5194/essd-2019-97
Preprint. Discussion started: 17 June 2019

Open Access Earth System Science Data Discussions

**Table 1: Characteristics of the plots**

| Name | A1 | A2 | A3 | A4 | B1 | B2 | C1 | C2 | C3 | D1 | D2 | D3 | E1 | E2 | F1 | F2 | G1 | G2 | H1 | H2 | H3 | H4 |
|---|---|---|---|---|---|---|---|---|---|---|---|---|---|---|---|---|---|---|---|---|---|---|
| Cluster | A | A | A | A | B | B | C | C | C | D | D | D | E | E | F | F | G | G | H | H | H | H |
| Surface type$_1$ | lawn | CCP | GP | CCP | NP | lawn | DCP | DCP | bushes | NP | NP | NP | NP | NP | NP | NP | DCP | CCP | DCP | CCP | CCP | lawn |
| Sealing degree [%]$_2$ | 0 | 93 | 54 | 92 | 83 | 0 | 89 | 73 | 0 | 80 | 81 | 86 | 76 | 75 | 76 | 78 | 86 | 97 | 85 | 94 | 92 | 0 |
| Build [year] | - | 1999 | 1999 | 1999 | 2011 | - | 2004 | 2004 | - | 1998 | 1998 | 1998 | 1999 | 1999 | 2014 | 2014 | 1987 | 1987 | 1985 | 1985 | 1985 | - |
| Height paving layer [cm] | - | 8 | 10 | 8 | 8 | - | 8 | 10 | - | 10 | 8 | 12 | 10 | 10 | 10 | 10 | 10 | 10 | 10 | 10 | 10 | - |
| Joint condition [cat.] | - | 3 | 2 | 3 | 0 | - | 1 | 1 | - | 1 | 1 | 1 | 2 | 2 | 0 | 0 | 3 | 3 | 2 | 2 | 2 | - |
| Joint material | - | sand | vegetated gravel-sand | sand | gravel-sand | - | gravel-sand | gravel-sand | - | mortar | gravel-sand | gravel-sand | mortar | mortar | mortar | mortar | sand | sand | sand | sand | sand | - |
| Joint vegetal cover [cat.] | - | 2 | 3 | 3 | 0 | - | 2 | 3 |  | 0 | 0 | 0 | 3 | 2 | 1 | 0 | 2 | 0 | 2 | 2 | 2 | - |
| Mean joint depth [mm] | - | 2 | 9 | 2 | 11 | - | 2 | 14 | - | 10 | 12 | 24 | 10 | 11 | 4 | 3 | 4 | 5 | 5 | 3 | 6 | - |
| Installation method$_3$ | profile wall | profile wall | profile wall | profile wall | filled | profile wall | filled | filled | profile wall | profile wall | profile wall | profile wall | filled | filled | filled | filled | filled | filled | filled | filled | filled | profile wall |

Subsurface$_4$

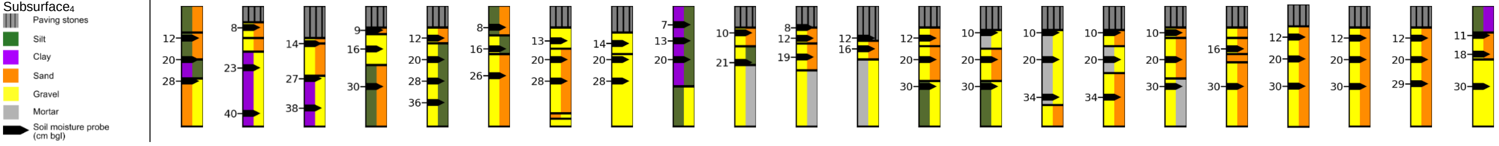

1: Abbreviations of surface types follow the classification of Timm et al. (2018) with CCP: classical concrete paving stones; DCP: designed concrete paving stones; GP: grass pavers; NP: natural paving stones.

2: The sealing degree equals 100% minus the joint proportion [%].

3: Sensors were installed with 2 different methods. Either they were installed in the undisturbed profile wall (profile wall) or in the excavated hole which then was filled from the top (filled)

4: The profiles show the 2 soil components with the biggest share. Minor components are not visualized. All profiles are presented to a uniform depth of 45 cm, although not all plots were excavated till this depth. In this case, the lowest layer encountered was extrapolated until the depth of 45 cm for illustration purposes. In case of installation method "filled", the depicted soil layers show the encountered soil material during excavation instead of the bedding material used for refilling.

### 3.4 Soil moisture and temperature measurements

Soil moisture and $T_{soil}$-measurements were carried out in 10 min intervals by the SMT100 sensors, which belong to the family of time domain transmission sensors (Qu et al., 2013). The SMT100 sensor operates by inducing a steep pulse to a closed transmission line of known length (Bogena et al., 2017). Thereby, the travel time of the pulse along the transmission line depends on the dielectric properties of the surrounding soil and forms the basis for water content measurements (Topp et al., 1980). Instead of measuring the travel time directly, the SMT100 measures an oscillation frequency, which is directly related to travel time (Qu et al., 2013). According to Bogena et al. (2017) it accounts around 150 MHz in water and 300 Hz in air. The sensor internally transforms the measured oscillation frequency into the dielectric permittivity ($\varepsilon_c$) (Bogena et al., 2017) and afterwards applies the Topp equation (Topp et al., 1980) to derive the volumetric water content ($\theta$). According to the manufacturer, the resolution of the SMT100 is at least 0.1 vol.% for $\theta$ and 0.01°C for $T_{soil}$. The accuracy in determining absolute values is 3 vol.% for $\theta$ (without soil specific calibration of the sensors) and between 0.2°C and 0.4°C for $T_{soil}$. Variables measured by the SMT100 represent average values over the entire sensor length of 10 cm. Measurements below PPs should therefore integrate substrates lying below joints as well as substrates lying below paving stones.

Temperature affects electromagnetic soil moisture measurements in various ways (Kapilaratne and Lu, 2017; Or and Wraith, 1999; Qu et al., 2013). Thereby, we observed strong temperature oscillations beneath the PPs with amplitudes reaching 20°C/day and extreme values ranging between -6°C and 47°C. These strong thermal variations affected the soil moisture measurements notably and called for a temperature correction of $\theta$. We therefore applied 3 different correction methods which are described in detail in the following.

First, we used the Complex Refraction Index Model (CRIM) model of Roth et al. (1990) (eq. 1) to consider the temperature-dependency of liquid water permittivity ($\varepsilon_w$) (eq. 2) (Handbook of Physics and Chemistry, 1986 as cited by Roth et al., 1990).

$$\theta = \frac{\varepsilon_c^\alpha - \varepsilon_s^\alpha - \phi(\varepsilon_a^\alpha - \varepsilon_s^\alpha)}{\varepsilon_w^\alpha - \varepsilon_a^\alpha} \qquad \text{(eq. 1)}$$

$$\epsilon_\mathrm{w}(\mathrm{T}_W) = 78.54\,[1 - 4.579 * 10^{-3}\,(\mathrm{T}_{soil} - 25) + 1.19 * 10^{-5}\,(\mathrm{T}_W - 25) - 2.8 * 10^{-8}(\mathrm{T}_W - 25)^3] \qquad \text{(eq. 2)}$$

Parameter values for eq. 1 were taken from Roth et al. (1990) with a geometry factor ($\alpha$) of 0.46 and a temperature independent permittivity of the gaseous ($\varepsilon_a$) and the solid phase ($\varepsilon_s$) of 1.0 and 3.9 respectively. The porosity ($\phi$) is derived in chapter 5 to account 0.37 (median of all plots). In eq. 2, we used $T_{soil}$ as a proxy for the water temperature ($T_w$).

Afterwards, the calculated $\theta$-values were aggregated to hourly values and the data-driven temperature correction method of Kapilaratne and Lu (2017) was applied. Although, this reduced temperature-induced $\theta$-oscillations noticeably, they were still present during periods with low saturation. Therefore, we used linear interpolation between daily minima for further correcting $\theta$. The linear interpolation was applied only for dry periods and thereby started 24 h after the ending of antecedent rain events. Together, the 3 methods turned out to be effective in removing temperature-induced $\theta$-fluctuations. Furthermore, times with frozen soils were removed from the $\theta$-time series (but not from the $\varepsilon_c$ time series), since freezing hinders vertical water movement within the profile. We therefore removed times where measured $T_{soil}$-values were below 0.5°C at any point in the profile or frozen joints were observed visually. For users who want to apply a different temperature correction scheme, the original $\varepsilon_c$ data is included within the dataset. Another source of error in $\theta$ may arise from salt spreading during winter road maintenance. This potentially leads to seasonal changes of soil salinity which in turn effects $\varepsilon_c$ (Ekblad and Isacsson, 2007). As electrical conductivity is not measured by the SMT100 sensor, it was neither possible to quantify the impact, nor to correct for.

Values reported in literature for the saturated water content ($\theta_s$) of base and bedding layers of PPs range between 20-45 vol.% (Brunetti et al., 2016; Illgen et al., 2007; Kodešová et al., 2014). As it is one of the main functions of PPs to drain infiltrating water rapidly to the subsurface, we expect $\theta$ to recede fast after ending infiltration and to hardly ever reach $\theta_s$. In contrast, at PPs with low permeability of underlying soils and missing or malfunctioning underdrains, we expect recorded $\theta$-values to reach $\theta_s$ and afterwards to recede slowly. Based on this, we classified the drainage behavior observed at the PPs into the categories “free drainage” and “restricted drainage”. This was done by a combination of visually characterizing the $\theta$-time series and by analyzing the empirical frequency distribution of $\theta$ recorded during rain events. In case of flashy behavior and low frequency of high $\theta$-values, the drainage behavior was classified as “free drainage”, while it was classified as “restricted drainage” if $\theta$-values recorded during rainfall were frequently in the range of $\theta_s$-values reported in literature.

To analyze the hydrologic behavior of different urban surface covers, we compared the $\theta$-dynamics recoded at different plot categories. Therefore, we calculated a mean $\theta$-time series for the categories “vegetated”, “PPs with free drainage” and “PPs with restricted drainage”. Thereby, times with data-gaps at any of the sensors were excluded, as gaps cause jumps in the calculated mean. Furthermore, the plots of cluster C are not included in the comparison, as the measurements at this cluster ended in Jan 2018 due to construction works.

### 3.5 Infiltration experiments

Infiltration experiments under falling head conditions were performed in spring 2016 on the plots. Therefore, we used double-ring infiltrometers with diameters of 320 mm and 556 mm of the inner and the outer ring, respectively. Bentonite was used to form a tight seal between the pavement layer and the infiltrometer. Figure 5 shows the performance of the infiltration experiments at the plots of cluster D.

**Figure 5: Infiltration experiments at the plots of cluster D**

Ponding depth was around 12.5 cm at the beginning of the experiments and water tables were recorded continuously during the experiment using pressure sensors and visual observations. Refilling occurred when water tables fall below 0.5 cm. Experiments were performed over 45 min except on plots with high infiltration rates, as the water supply was limited to 200 L at most of the plots. As expected, infiltration rates were higher at the beginning of the experiment (initial infiltration rates) and decreased over time until they reached a constant rate (final infiltration rate). The main cause for this decline is the decrease of matrix suction gradients with the proceeding of the infiltration front (Hillel, 1998).

### 3.6 Derivation of soil hydrological parameters

Depending on the drainage behavior, the $\theta$-measurements were used to either derive $\theta_s$ (for PPs with restricted drainage) or to derive $\theta_{fc}$ (for PPs with free drainage). For PPs with free drainage, we used the median of all $\theta$-values recorded in the period 48-72 h after rain events to estimate $\theta_{fc}$. To ensure that soils were initially wetted above $\theta_{fc}$, only events with a precipitation sum of at least 10 mm were considered for assessing $\theta_{fc}$. At PPs with restricted drainage, saturation was reached frequently during rainfall. We used the 0.99 quantile of $\theta$ measured during rain events to assess $\theta_s$ of these plots, which is assumed to equal $\phi$. As $\theta$ calculated with the CRIM model (eq. 1) depends on $\phi$, we used $\theta$ calculated with the $\phi$-independent Topp equation (Topp et al., 1980) to derive $\theta_s$.

The Philip infiltration model (Philip, 1957) (eq. 3) was used to describe the cumulative infiltration ($I$) measured during the infiltration experiments.

$$I = St^{\frac{1}{2}} + At \qquad \text{(eq. 3)}$$

where $S$ is the sorptivity, $t$ is time and $A$ is a parameter representing the theoretical minimum of the infiltration rate (approached asymptotically for large values of $t$) which is defined as endinfiltration rate. The two model parameters $S$ and $A$, as well as their confidence intervals were determined inversely, by fitting the model to the observed $I$ using the least-square optimization algorithm implemented in the Python module SciPy (function optimize.curve_fit). After determining the parameters, we used the fitted Philip model to calculate the mean infiltration rate over a period of 5 h, which we defined as infiltration capacity ($i_{cap}$). The duration of 5 h represents the median duration of the 302 separated rainfall events within the study period. In addition, we assessed the initial infiltration rate ($i_{start}$) by calculating the mean infiltration rate over the first 10 min of infiltration. By calculating $i_{cap}$ and $i_{start}$ with parameter values located at the boundary of their confidence intervals, we determined the uncertainties of $i_{cap}$ and $i_{start}$. Finally, the depression storage of joints ($S_{joints}$) was assessed by multiplying the mean joint depth by the joint proportion (Table 1).

## 4. Data

### 4.1 Soil moisture

Most of the studied PPs indicate free drainage, as $\theta$ recedes fast after the end of a precipitation event. In contrast, 6 of the 18 studied PPs (plots of cluster H, B and C) revealed restricted drainage, as $\theta$ often reached a plateau during rainfall which persisted even after the end of a precipitation event. At the plots of cluster H restricted drainage was apparent at all sensors, while it was mainly limited to lower layers at the plots of clusters B and C. Figure 6 shows the depth-dependent comparison between $\theta$ measured at vegetated plots, PPs with free drainage and PPs with restricted drainage, while Table 2 gives an overview on the number of sensors included within each category.

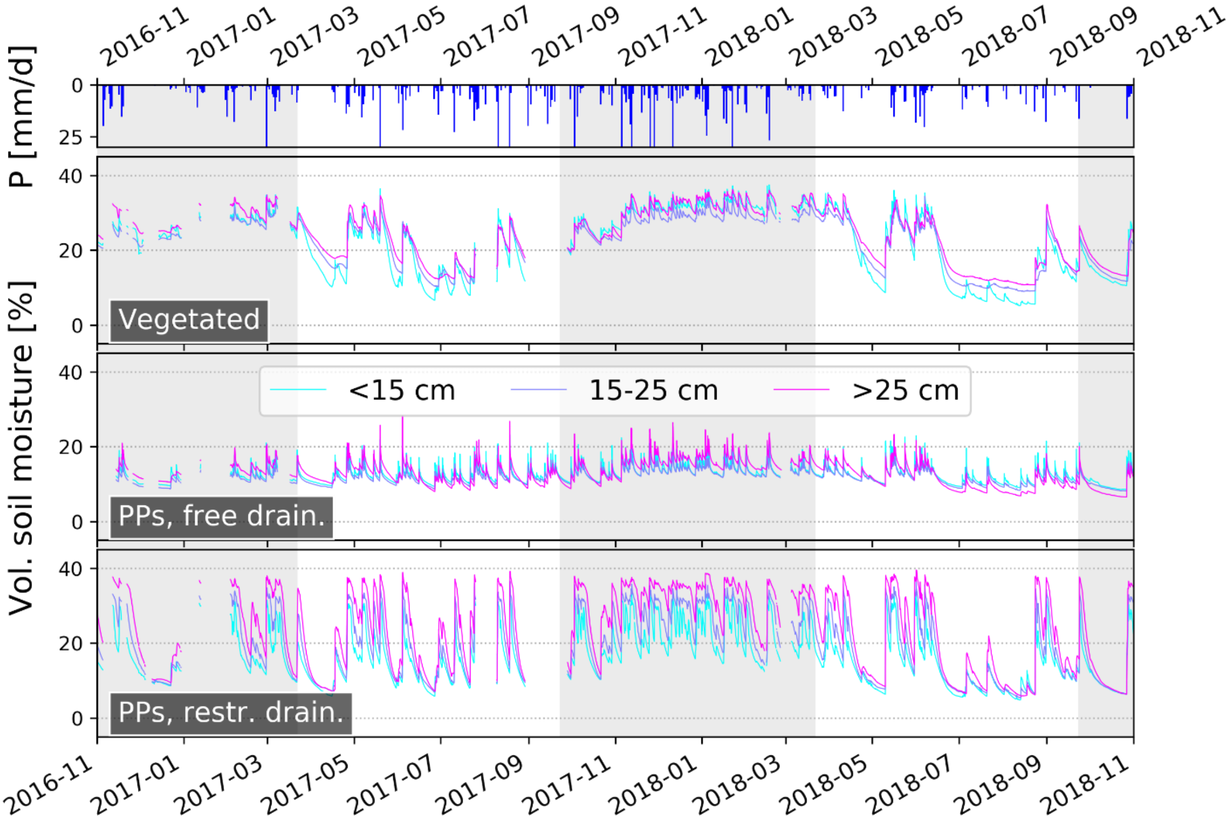

**Figure 6: Mean $\theta$ of the vegetated surfaces (top), PPs with free drainage (middle) and PPs with restricted drainage (bottom). The grey background indicates the winter half year.**

**Table 2: Number of sensors included within each category Figure 6**

| | Depth below ground surface | | |
|---|---|---|---|
| | **<15 cm** | **15-25 cm** | **>25 cm** |
| **Vegetated** | 3 | 3 | 3 |
| **PPs with free drainage** | 13 | 11 | 10 |
| **PPs with restricted drainage** | 4 | 4 | 5 |

Recorded $\theta$-time series of PPs differ substantially from those of vegetated surfaces. At the vegetated plots, recoded $\theta$-values show a seasonal pattern with a wet state occurring during the winter half year. During the wet state, $\theta$ is similar in all depths while the upper layers dry out faster and stronger during summer. A further depth-dependency is apparent, as the dampening and delay of the $\theta$-rise increases with depth. In contrast, PPs with free drainage show hardly any seasonal and depth-dependent differences. Rise and recession of $\theta$ occurs very fast and reveals a high "flashiness" of the soil water storage. In contrast, PPs with restricted drainage show depth-dependent differences, as plateaus in $\theta$ are more persistent and appear more frequent at greater depths. Furthermore, a wet state can be identified, as $\theta$ recedes seldom in winter.

One of the main functions of PPs is to drain infiltrating water rapidly to the subsurface and hence to avoid temporary saturation. The flashiness of the soil water storage observed at PPs with free drainage indicates that these plots fulfil this function. In contrast, the plateaus apparent in $\theta$ recorded at PPs with restricted drainage indicate that soils were often saturated. Possible effects are the formation of saturation overland flow as well as impacts on the bearing capacity and the frost-resistance. This shows the relevancy of the permeability of underlying soils which is in contrast to the findings of numerical studies reporting limited influence of deeper layers on the hydrologic performance of PPs (Brunetti et al., 2016; Illgen et al., 2007). The difference between plots with free drainage and plots with restricted drainage gets apparent when regarding the empirical frequency distribution of $\theta$-values recorded during rain events (Figure 7).

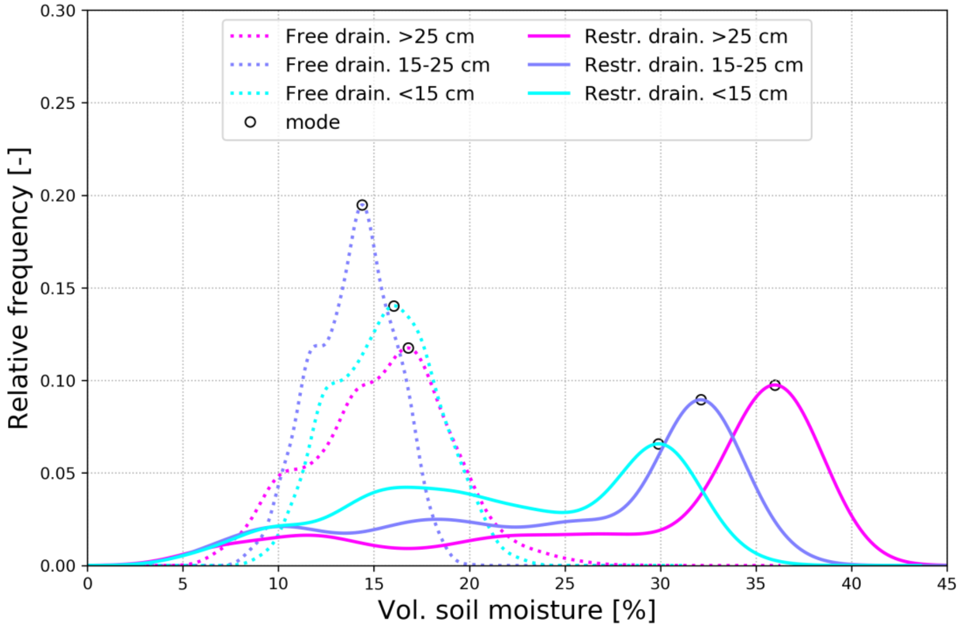

**Figure 7: Density distribution of $\theta$-values measured at PPs during rain events depending on drainage behavior and sensor depth. Depicted densities are mean values of all sensors within each category.**

During rain events, $\theta$-values are much lower on PPs with free drainage and values above 25 vol.% are hardly ever reached. In contrast, $\theta$-values measured on PPs with restricted drainage are frequently above 25 vol.% during rain events. As bedding and base layers are technical substrates with defined hydrologic properties, the porosities of all PPs should be similar. The frequency distribution recorded at PPs with free drainage indicates that these plots hardly ever reached saturation within the study period. Therefore, infiltration excess overland flow is the only process leading to surface runoff on PPs with free drainage.

### 4.2 Soil temperatures ($T_{soil}$)

The recorded $T_{soil}$-values show periodic variations at the diurnal and at the annual scale. Figure 8 shows the mean of the measured $T_{soil}$-values for different depths for PPs and vegetated surfaces.

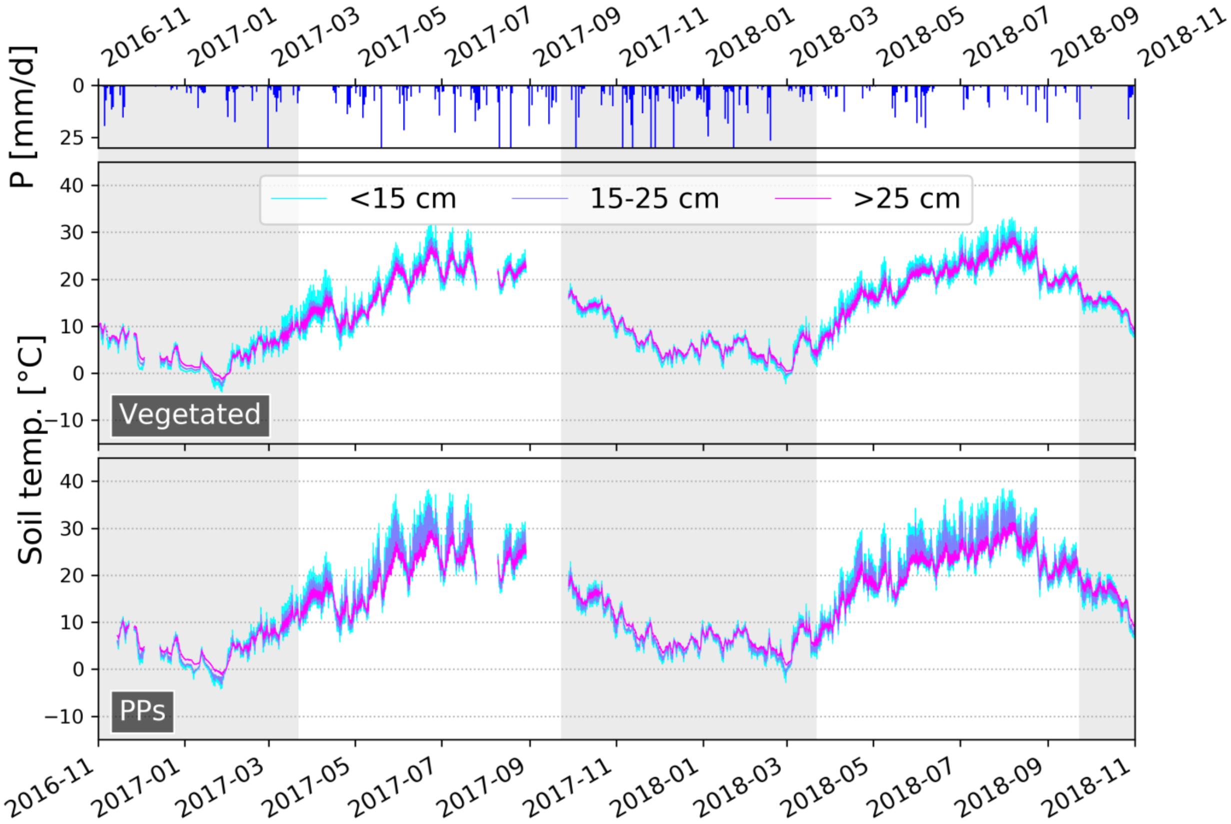

5 **Figure 8: Mean soil temperatures measured in different depths for vegetated (top) and paved surfaces (bottom). The grey background indicates the winter half year.**

Both diurnal and annual amplitudes are more pronounced on PPs than on vegetated plots. Differences are mostly pronounced during the summer half year, when PPs undergo a much stronger diurnal heating. This is also reflected in the recorded maxima $T_{soil}$-values, which are 37°C on vegetated and 47°C on PPs. The heterogeneity of urban structures causes a high spatial variability of the climatic input and therefore is a major influence on $T_{soil}$-values. Highest $T_{soil}$-values were recorded at cluster D, which is located close to a south-orientated facade of an east-west orientated urban canyon within the city center. In contrast, maxima soil $T_{soil}$-values recorded at the shaded Cluster A were around 17°C lower. Another characteristic of cluster A is the similarity of $T_{soil}$-values between vegetated and paved plots. Cluster H is located in a residential area and is only partially shaded by surrounding objects. Due to the exposure to direct solar irradiation, the differences between vegetated and paved plots are much more pronounced at this cluster (Figure 9).

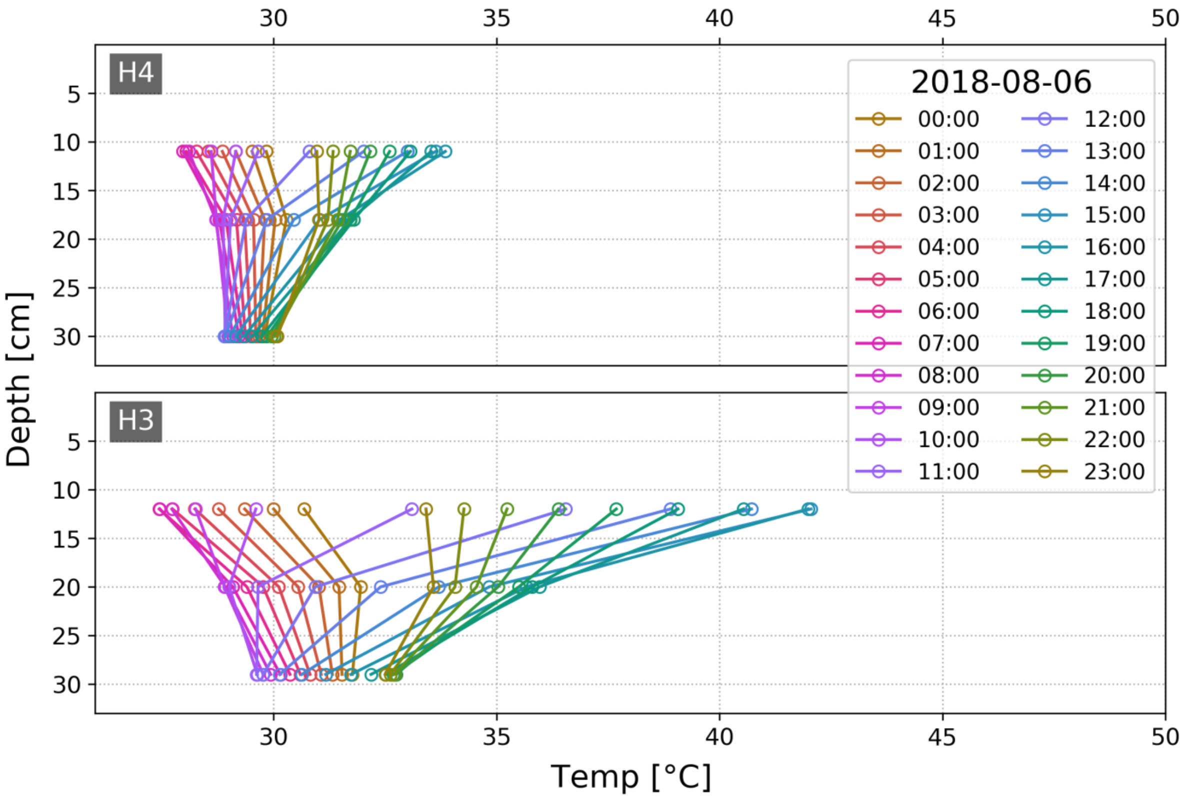

**Figure 9: Diurnal temperature cycle measured at the vegetated plot H4 (top) and the paved plot H3 (bottom) on August 6th 2018**

Figure 9 shows that the diurnal $T_{soil}$-amplitude is strongest at the uppermost sensors and dampened with depth. The diurnal amplitude in 30 cm depth is higher at the paved plot, indicating a higher penetration depth of $T_{soil}$-fluctuations at this plot. This is mainly caused by higher surface temperatures, but furthermore integrates different thermal properties. The $T_{soil}$-depth profiles offer the opportunity to derive ground surface temperatures and the penetration depth of periodic temperature variations and can further be used to calculate ground heat fluxes.

### 4.3 Infiltration experiments

Infiltration experiments were performed at all PPs except at the plots E2, F2 and H3. The plots E1 and E2 are equal in terms of joint properties and proportions, which leads to the assumption that infiltration measured at E1 might be applied as representative for E2. The same applies to the plots F1 and F2. Figure 10 shows the data of the infiltration experiments together with the fitted Philip infiltration model (eq. 3).

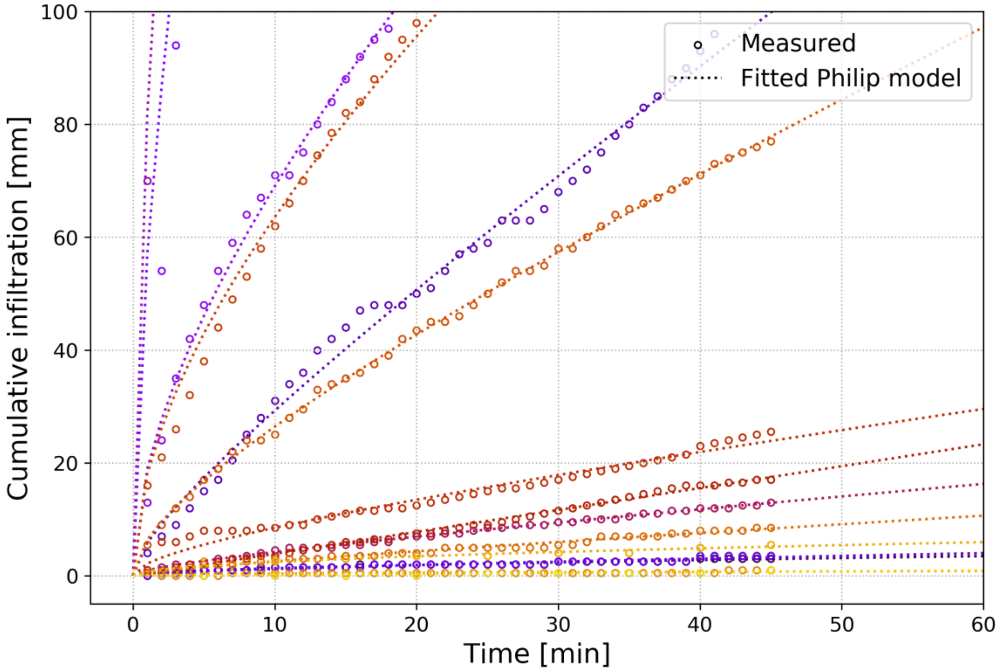

**Figure 10: Measured infiltration and simulation with the Philip infiltration model.**

## 5. Derived soil hydrological parameters

The measurements were used to derive soil hydrological parameters of the PPs. Depending on the drainage behavior of the PPs, the $\theta$-measurements were either used to derive $\theta_{fc}$ or $\theta_s$. Data of the infiltration experiments was used to derive the parameters $S$ and $A$ of the Philip infiltration model which in turn were used to derive $i_{cap}$ and $i_{start}$. The depression storage of joints ($S_{joints}$) was assessed from the mean joint depth and the joint proportion. Table 3 shows the derived hydrological parameters for the PPs.

**Table 3: Derived hydrologic parameters for the PPs. The parameters $\theta_{fc}$ and $\theta_s$ are shown for three different depth ranges, while the remaining parameters are provided independent of depth. The *A*- parameter is considered as endinfiltration rate.**

| | $\theta_{fc}$ [vol.%] | | | $\theta_s$ [vol.%] | | | $S$ [mm/min$^{1/2}$] | $A$ [mm/min] | $i_{cap}$ [mm/h] | $i_{start}$ [mm/h] | $S_{joints}$ [mm] |
|---|---|---|---|---|---|---|---|---|---|---|---|
| | <15 cm | 15-25 cm | >25 cm | 15-25 cm | <15 cm | >25 cm | | | | | |
| **A2** | 9.91 | 18.11 | 29.47 | - | - | - | 0.39 ± 0.02 | 0.01 ± 0.00 | 1.79 ± 0.36 | 7.86 ± 0.75 | 0.14 |
| **A3** | 11.88 | - | 14.94 | - | - | - | 4.23 ± 0.42 | 1.59 ± 0.08 | 109.92 ± 6.27 | 175.57 ± 12.80 | 5.04 |
| **A4** | 14.64 | 10.94 | 12.31 | - | - | - | 0.29 ± 0.04 | 0.03 ± 0.01 | 2.73 ± 0.57 | 7.27 ± 1.18 | 0.16 |
| **B1** | - | - | - | 36.72 | 36.76 | 39.37 | 47.04 ± 1.33 | 9.85 ± 0.26 | 754.25 ± 20 | 1483.86 ± 41 | 1.87 |
| **C1** | - | - | - | 38.53 | 36.51 | 40.2 | 17.60 ± 0.40 | 1.34 ± 0.08 | 141.19 ± 6.21 | 414.10 ± 12.42 | 0.22 |
| **C2** | - | - | - | 36.02 | 38.35 | 36.81 | 66.55 ± 5.65 | 15.05 ± 2.37 | 1133.29 ± 166 | 2165.48 ± 250 | 3.78 |
| **D1** | 10.2 | 15.7 | - | - | - | - | 0.79 ± 0.03 | 0.17 ± 0.01 | 12.89 ± 0.47 | 25.13 ± 0.98 | 2 |
| **D2** | 14.54 | 13.7 | - | - | - | - | 0.00 ± 0.06 | 0.39 ± 0.01 | 23.29 ± 0.88 | 23.29 ± 1.84 | 2.28 |
| **D3** | 14.94 | 16.28 | - | - | - | - | 1.91 ± 0.17 | 0.25 ± 0.03 | 21.37 ± 2.48 | 50.99 ± 5.16 | 3.36 |
| **E1** | 12.58 | 10.63 | 11.88 | - | - | - | 17.04 ± 0.45 | 0.97 ± 0.08 | 117.14 ± 6.41 | 381.39 ± 13.34 | 2.4 |
| **E2** | 18.15 | 11.55 | 9.18 | - | - | - | - | - | - | - | 2.75 |
| **F1** | 11.33 | 7.11 | 11.9 | - | - | - | 5.46 ± 0.11 | 0.92 ± 0.02 | 73.85 ± 1.57 | 158.50 ± 3.26 | 0.96 |
| **F2** | 11.62 | 8.95 | 10.7 | - | - | - | - | - | - | - | 0.66 |
| **G1** | 11.7 | 13.9 | 14.19 | - | - | - | 0.41 ± 0.05 | 0.12 ± 0.01 | 8.90 ± 0.73 | 15.21 ± 1.52 | 0.56 |
| **G2** | 10.94 | 10.62 | 15.43 | - | - | - | 0.11 ± 0.02 | 0.00 ± 0.00 | 0.37 ± 0.36 | 2.02 ± 0.74 | 0.15 |
| **H1** | - | - | - | 36.46 | 36.22 | 37.3 | 0.77 ± 0.14 | 0.00 ± 0.03 | 2.65 ± 2.00 | 14.53 ± 4.20 | 0.75 |
| **H2** | - | - | - | 36.04 | 36.6 | 35.94 | 0.00 ± 0.07 | 0.02 ± 0.01 | 0.93 ± 1.00 | 0.93 ± 2.09 | 0.18 |
| **H3** | - | - | - | 36.34 | 35.25 | 36.01 | - | - | - | - | - |
| **Median** | **11.79** | **11.55** | **12.31** | **36.4** | **36.56** | **37.06** | **0.78 ± 0.09** | **0.21 ± 0.02** | **17.13 ± 1.28** | **24.21 ± 2.68** | **0.96** |

The calculated $\theta_{fc}$-values range between 7 vol.% and 29 vol.%, with values above 20 vol.% only occurring at plot A2 in 40 cm depths. The median of the calculated $\theta_{fc}$-values is similar within all depth ranges and the median of all sensors accounts 12 vol.%. The median of the obtained $\theta_s$-values accounts 36 vol.% for sensors located in bedding layer and 37 vol.% for sensors located in the base layers. Obtained $\theta_s$-values are within the range reported in literature. Illgen (2009) obtained $\theta_s$-values of 45% (base layer) and 37% (bedding layer) by calibration of the HYDRUS-2D model with lysimeter data. Similarly, Brunetti et al. (2016) used a particle swarm optimization algorithm to calibrate HYDRUS-1D. They obtained $\theta_s$-values of 30% and 20% for the bedding and the base layer respectively (single porosity model). Multistep outflow experiments were performed by Kodešová et al. (2014) leading to $\theta_s$-values of 42% and 43% for the bedding and base layer respectively. As bedding and base layers are technical substrates introduced during the construction of PPs, we assume the derived values for $\theta_s$ and $\theta_{fc}$ to be representative also for other PPs.

Values obtained for $i_{cap}$ range between 0.37 mm/h and 1133 mm/h. According to national regulations, PPs must show a minimum $i_{cap}$ of 97.2 mm/h (Borgwardt, 2001). The derived $i_{cap}$-values show that only 5 of the 15 tested PPs satisfy this requirement. Values below 2 mm/h were obtained for the plots A2, G2 and H2 which are characterized by a low proportion of joints and a bad joint condition. Clogging was shown to take place mainly within the first years after the installation of PPs (Boogaard et al., 2014; Borgwardt, 2006; Lucke and Beecham, 2011). As the age of all plots (except the plots of cluster F) lie between 14-20 years, all plots are expected to be affected by clogging. Fassman and Blackbourn (2010) highlight the role of adjacent land use on clogging. All 3 plots with lowest $i_{cap}$ are located in close vicinity to urban greenspaces and trees. This might explain the low $i_{cap}$-values observed at these plots. Infiltration characteristics of the 2 PPs with mortar filled joints (E1 and F1) are similar, despite the differences in their age and joint condition. While the mortar filled joints of plot E1 were classified as “bad”, they were classified as “very good” on plot F1. Nevertheless, the bad joint condition of plot E1 is caused by broken and crumbly joint mortar which may explain the higher $i_{cap}$ of this plot compared to plot F1. It therefore seems that the aging of the joint mortar of plot E1 resulted in cracks compensating the clogging of the mortar matrix.

## 6. Data availability

The dataset is available at the FreiDok plus data repository at https://freidok.uni-freiburg.de/data/149321 and https://doi.org/10.6094/UNIFR/149321 (Schaffitel et al., 2019) and contains time series of $\theta$, $T_{soil}$, $\varepsilon_c$ and climate data measured at the WBI station. Furthermore, $et_0$ calculated for the WBI climate station and the separation of wet dry cycles is included. The $\theta$-time series is provided with an hourly resolution and includes the temperature correction procedures described in chapter 3.4. For users who need $\theta$ with a higher temporal resolution, or want to apply different temperature correction schemes than described in chapter 3.4, $\varepsilon_c$ is provided with a 10 min temporal resolution. Soil temperature is also provided with a temporal resolution of 10 min. The event classification is provided with hourly resolution, while $et_0$ is provided with both - daily and hourly resolution. Online sources for the data of the climate stations depicted in Figure 1 are listed in

Table 4, while meteorological data for the WBI station with a temporal resolution of 10 min is included in the dataset.

**Table 4: Sources of climate data for the study area**

| **Station** | **Temporal resolution** | Source |
|---|---|---|
| **DWD** | 10 min (free download), 1 min (fee-based) | ftp://ftp-cdc.dwd.de/pub/CDC/observations_germany/climate/ |
| **WBI** | 1 h (free download) ; 10 min (on request) | http://www.wetter-bw.de/Internet/AM/NotesBwAM.nsf/bwweb/fa31cce8b142f059c1257ca7003c9ed1?OpenDocument |
| **Vaub** | 10 min (free download); 1 min (on request) | Link "Vauban Meteo Station"on http://hydro.uni-freiburg.de/strt-en?set_language=en |
| **Uni** | 1 min (free download) | https://weather.uni-freiburg.de/ |

Furthermore, the original data of the infiltration experiments is provided. Sensor and plot specific meta-information is supplied in two separate files. All hydrologic parameters derived within this study are included in these files. A readme file contains information on the organization of all folders and files.

## 7. Summary and conclusions

We provide a unique dataset of soil moisture and soil temperatures measured within an urban environment. So far, only few studies conducted measurements within urban soils and there is a need for more observations (Salvadore et al., 2015). The analysis of the soil moisture contents revealed important information on the behavior of permeable pavements within the urban environment. Recorded soil moisture contents revealed restricted drainage to occur on 6 of the studied 18 permeable pavements, leading to temporary saturation in the subsurface of this plots. This contradicts the results of previous simulation studies which revealed little importance to the permeability of lower lying soil layers (Brunetti et al., 2016; Illgen et al., 2007). The observed water saturation potentially affects the bearing capacity and frost-resistance of the pavements, but may also lead to the formation of saturation overland flow. We used the times with saturation to derive the saturated water content and the porosity of these plots. The median of the derived saturated water contents accounts 37 vol.%. The remaining 12 permeable pavements revealed free drainage and showed fast soil moisture recession after rainfall events. This flashiness causes that saturation is hardly ever reached and that neither pronounced seasonal nor depth-dependent differences appear in soil water contents. The infiltration capacity of these pavements is restricted only by the properties of their joints and surface runoff generation is limited to infiltration excess overland flow. Measured soil moisture contents were used to derive the field capacity of base and bedding layers. The median of the obtained field capacities accounts 12 vol.% and is similar for all depths. As base and bedding layers are technical substrates with defined hydrological properties, the derived saturated water contents and field capacities should be representative for other permeable pavements. In addition to soil moisture and temperature measurements, infiltration experiments were performed on 15 of the permeable paved plots and used to derive their infiltration capacity. The results showed that only 5 of the studied permeable pavements fulfilled national regulations. Lowest infiltration capacities were obtained for pavements with small proportions of joints and high degree of surface clogging. The methods used to derive soil hydrological parameters proved their ability, as all parameters lie within the range reported in literature.

Recorded soil temperatures revealed greater temperature variations under permeable pavements compared to vegetated surfaces. Thereby, differences are most pronounced during the summer, when pavements undergo a stronger heating during daytime. Our measurements further indicate that the penetration depth of temperature variations is higher on paved plots compared to vegetated plots. Besides the surface type, the surrounding urban fabric is a main control of soil temperatures. While soil temperatures reached 47°C on a paved plot exposed to direct solar irradiation, recorded maximum temperatures were 17°C lower at a shaded pavement. Furthermore, surface shading reduces the temperature difference between vegetated and paved plots. While the temperature difference is pronounced at clusters exposed to direct solar irradiation, it is marginal at shaded clusters.

The provided dataset and the parameters derived within this study are valuable for various purposes. One possible application is the usage for calibration and validation of urban hydrological and climatological models. Further applications include the derivation of water and energy fluxes. Hence, the dataset enables to study the role of permeable pavements within urban storm water management practices. Furthermore, we encourage its usage to analyze the ground heat flux of urban areas. This might be of special interest for studying the urban energy balance but also for analyzing urban subsurface heat islands. Usage of the data is not only limited to the fields of urban hydrology and climatology, but also may be of interest for urban planning and geoengineering. Against this background, we are convinced that the provided dataset is of great value for various disciplines and scientific issues.

## Authors contribution

AS designed and maintained the sensor network and prepared the manuscript with contributions of all co-authors.

## Acknowledgements

This study is part of the research project WaSiG (Wasserhaushalt siedlungsgeprägter Gewässer) which is part of joint project ReWaM (Regionales Wasserressourcen-Management für den nachhaltigen Gewässerschutz in Deutschland) funded by the German Ministry of Education and Research (BMBF). Furthermore, this work was supported by the badenova AG and Co. KG (innovation fund for the protection of climate and water). Besides, we are greatly indebted to the local civil construction authority (Garten- und Tiefbauamt Freiburg i.Br.), who supported us during the installation of the soil moisture sensors. Furthermore, we want to thank the Center for Agricultural Technology Augustenberg and the State Viniculture Institute Freiburg for providing data for the WBI climate station. Finally, we like to express our gratitude to Caroline Siebert for performing most of the infiltration experiments.

## Literature

Allen, R. G., Pereira, L. S., Raes, D. and Smith, M.: Crop evapotranspiration - Guidelines for computing crop water requirements, Rome, Italy., 1998.

Andersen, C. T., Foster, I. D. L. and Pratt, C. J.: The role of urban surfaces (permeable pavements) in regulating drainage and evaporation: Development of a laboratory simulation experiment, Hydrol. Process., 13(4), 597–609, doi:10.1002/(SICI)1099-1085(199903)13:4<597::AID-HYP756>3.0.CO;2-Q, 1999.

Bogena, H. R., Huisman, J. A., Schilling, B., Weuthen, A. and Vereecken, H.: Effective calibration of low-cost soil water content sensors, Sensors (Switzerland), 17(1), doi:10.3390/s17010208, 2017.

Boogaard, F., Lucke, T., van de Giesen, N. and van de Ven, F.: Evaluating the infiltration performance of eight dutch permeable pavements using a new full-scale infiltration testing method, Water (Switzerland), 6(7), 2070–2083, doi:10.3390/w6072070, 2014.

Borgwardt, S.: Merkblatt für wasserdurchlässige Befestigungen von Verkehrsflächen (der Forschungsgesellschaft für Straßen- und Verkehrswesen - FGSV) Kommentierung mit ausführlichen Hinweisen für die Planung und Ausführung versickerungsfähiger Bauweisen mit Betonpflaster, Fachvereinigung Betonprodukte für Straßen-, Landschafts- und Gartenbau., 2001.

Borgwardt, S.: Long-Term In-Situ Infiltration Performance of Permeable Concrete Block Pavement, 8th Int. Conf. Concr. Block Paving, Novemb. 6-8, 2006 San Fr. Calif. USAnternational Conf. Concr. block paving, 149–160 [online] Available from: http://citeseerx.ist.psu.edu/viewdoc/download?doi=10.1.1.365.9174&rep=rep1&type=pdf, 2006.

Brocca, L., Melone, F. and Moramarco, T.: On the estimation of antecedent wetness conditions in rainfall-runoff modelling, Hydrol. Process., 22(5), 629–642, doi:10.1002/hyp.6629, 2008.

Brown, R. A. and Borst, M.: Quantifying evaporation in a permeable pavement system, Hydrol. Process., 29(9), 2100–2111, doi:10.1002/hyp.10359, 2015.

Brunetti, G., Šimůnek, J. and Piro, P.: A comprehensive numerical analysis of the hydraulic behavior of a permeable pavement, J. Hydrol., 540, 1146–1161, doi:10.1016/j.jhydrol.2016.07.030, 2016.

Cristiano, E., Veldhuis, M. C. Ten and Van De Giesen, N.: Spatial and temporal variability of rainfall and their effects on hydrological response in urban areas - A review, Hydrol. Earth Syst. Sci., 21(7), 3859–3878, doi:10.5194/hess-21-3859-2017, 2017.

Eagleson, P. S.: Climate, soil, and vegetation: 3. A simplified model of soil moisture movement in the liquid phase, Water Resour. Res., 14(5), 722–730, doi:10.1029/WR014i005p00722, 1978.

Ekblad, J. and Isacsson, U.: Time-domain reflectometry measurements and soil-water characteristic curves of coarse granular materials used in road pavements, Can. Geotech. J., 44(7), 858–872, doi:10.1139/t07-024, 2007.

Elliott, A. H. and Trowsdale, S. A.: A review of models for low impact urban stormwater drainage, Environ. Model. Softw., 22(3), 394–405, doi:10.1016/j.envsoft.2005.12.005, 2007.

Fassman, E. A. and Blackbourn, S.: Urban Runoff Mitigation by a Permeable Pavement System over Impermeable Soils, J. Hydrol. Eng., 15(6), 475–485, doi:10.1061/(ASCE)HE.1943-5584.0000238, 2010.

FGSV: Richtlinien für die Standardisierung des Oberbaus., 2012.

Fletcher, T. D., Andrieu, H. and Hamel, P.: Understanding, management and modelling of urban hydrology and its consequences for receiving waters: A state of the art, Adv. Water Resour., 51, 261–279, doi:10.1016/j.advwatres.2012.09.001, 2013.

Grimmond, C. S. B. and Oke, T. R.: An evapotranspiration-interception model for urban areas, Water Resour. Res., 27(7), 1739–1755, doi:10.1029/91WR00557, 1991.

Grimmond, C. S. B., Blackett, M., Best, M. J., Barlow, J., Baik, J. J., Belcher, S. E., Bohnenstengel, S. I., Calmet, I., Chen, F., Dandou, A., Fortuniak, K., Gouvea, M. L., Hamdi, R., Hendry, M., Kawai, T., Kawamoto, Y., Kondo, H., Krayenhoff, E. S., Lee, S. H., Loridan, T., Martilli, A., Masson, V., Miao, S., Oleson, K., Pigeon, G., Porson, A., Ryu, Y. H., Salamanca, F., Shashua-Bar, L., Steeneveld, G. J., Tombrou, M., Voogt, J., Young, D. and Zhang, N.: The international urban energy balance models comparison project: First results from phase 1, J. Appl. Meteorol. Climatol., 49(6), 1268–1292, doi:10.1175/2010JAMC2354.1, 2010.

Guo, R., Guo, Y. and Wang, J.: Stormwater capture and antecedent moisture characteristics of permeable pavements, Hydrol. Process., 32(17), 2708–2720, doi:10.1002/hyp.13213, 2018.

Hillel, D.: Environmental Soil Physics, Acad. Press, San Diego, Calif., 1998.

Illgen, M.: Das Versickerungsverhalten durchlässig befestigter Siedlungsflächen und seine urbanhydrologische Quantifizierung., 2009.

Illgen, M., Harting, K., Schmitt, T. G. and Welker, A.: Runoff and infiltration characteristics of pavement structures-review of an extensive monitoring program, Water Sci. Technol., 56(10), 133–140, doi:10.2166/wst.2007.750, 2007.

Kapilaratne, R. G. C. J. and Lu, M.: Automated general temperature correction method for dielectric soil moisture sensors, J. Hydrol., 551, 203–216, doi:10.1016/j.jhydrol.2017.05.050, 2017.

Kimball, B. A., Jackson, R. D., Nakayama, F. S., Idso, S. B. and Reginato, R. J.: Soil-heat flux determination: temperature gradient method with computed thermal conductivities, Soil Sci. Soc. Am. J., 40(1), 25–28, doi:10.2136/sssaj1976.03615995004000010011x, 1976.

Kodešová, R., Fér, M., Klement, A., Nikodem, A., Teplá, D., Neuberger, P. and Bureš, P.: Impact of various surface covers on water and thermal regime of Technosol, J. Hydrol., 519(PB), 2272–2288, doi:10.1016/j.jhydrol.2014.10.035, 2014.

Lahoz, W. A. and De Lannoy, G. J. M.: Closing the Gaps in Our Knowledge of the Hydrological Cycle over Land: Conceptual Problems., 2014.

Litvak, E., Manago, K. F., Hogue, T. S. and Pataki, D. E.: Evapotranspiration of urban landscapes in Los Angeles, California at the municipal scale, Water Resour. Res., 53(5), 4236–4252, doi:10.1002/2016WR020254, 2017.

LUBW: Wasser- und Bodenatlas Baden-Württemberg (WaBoA), Ministry of Environment Baden-Württemberg., 2012.

Lucke, T. and Beecham, S.: Field investigation of clogging in a permeable pavement system, Build. Res. Inf., 39(6), 603–615, doi:10.1080/09613218.2011.602182, 2011.

Menberg, K., Blum, P., Schaffitel, A. and Bayer, P.: Long-term evolution of anthropogenic heat fluxes into a subsurface urban heat island, Environ. Sci. Technol., 47(17), 9747–9755, doi:10.1021/es401546u, 2013.

Oke, T. R.: The urban energy balance, Prog. Phys. Geogr., 12(4), 471–508, doi:10.1177/030913338801200401, 1988.

Oke, T. R., Mills, G., Christen, A. and Voogt, J. A.: Urban Climates, Cambridge University Press, Cambridge., 2017.

Or, D. and Wraith, J. M.: Temperature effects on soil bulk dielectric permittivity measured by time domain reflectometry: A physical model, Water Resour. Res., 35(2), 371–383, doi:10.1029/1998WR900008, 1999.

Park, D. G., Sandoval, N., Lin, W., Kim, H. and Cho, Y. H.: A case study: Evaluation of water storage capacity in permeable block pavement, KSCE J. Civ. Eng., 18(2), 514–520, doi:10.1007/s12205-014-0036-y, 2014.

Philip, J. R.: The theory of infiltration: 4. Sorptivity and algebraic infiltration equations, Soil Sci., 84(3), 257–264, 1957.

Qu, W., Bogena, H. R., Huisman, J. A. and Vereecken, H.: Calibration of a Novel Low-Cost Soil Water Content Sensor Based on a Ring Oscillator, Vadose Zo. J., 12(2), 0, doi:10.2136/vzj2012.0139, 2013.

Ragab, R., Rosier, P., Dixon, A., Bromley, J. and Cooper, J. D.: Experimental study of water fluxes in a residential area: 2. Road infiltration, runoff and evaporation, Hydrol. Process., 17(12), 2423–2437, doi:10.1002/hyp.1251, 2003.

Razzaghmanesh, M. and Borst, M.: Investigation clogging dynamic of permeable pavement systems using embedded sensors, J. Hydrol., 557, 887–896, doi:10.1016/j.jhydrol.2018.01.012, 2018.

Roberts, S. M., Oke, T. R., Grimmond, C. S. B. and Voogt, J. A.: Comparison of four methods to estimate urban heat storage, J. Appl. Meteorol. Climatol., 45(12), 1766–1781, doi:10.1175/JAM2432.1, 2006.

Roth, K., Schulin, R., Flühler, H. and Attinger, W.: Calibration of time domain reflectometry for water content measurement using a composite dielectric approach, Water Resour. Res., 26(10), 2267–2273, doi:10.1029/WR026i010p02267, 1990.

Salvadore, E., Bronders, J. and Batelaan, O.: Hydrological modelling of urbanized catchments: A review and future directions, J. Hydrol., 529(P1), 62–81, doi:10.1016/j.jhydrol.2015.06.028, 2015.

Schaffitel, A., Schuetz, T. and Weiler, M.: A distributed soil moisture, temperature and infiltrometer dataset for permeable pavements and green spaces, FreiDok plus; available at: https://doi.org/10.6094/UNIFR/149321, https://freidok.uni-freiburg.de/data/149321, doi:10.6094/UNIFR/149321, 2019.

Schirmer, M., Leschik, S. and Musolff, A.: Current research in urban hydrogeology - A review, Adv. Water Resour., 51, 280–291, doi:10.1016/j.advwatres.2012.06.015, 2013.

Scholz, M. and Grabowiecki, P.: Review of permeable pavement systems, Build. Environ., 42(11), 3830–3836, doi:10.1016/j.buildenv.2006.11.016, 2007.

Shuster, W. D., Bonta, J., Thurston, H., Warnemuende, E. and Smith, D. R.: Impacts of impervious surface on watershed hydrology: A review, Urban Water J., 2(4), 263–275, doi:10.1080/15730620500386529, 2005.

Stander, E. K., Rowe, A. A., Borst, M. and O'Connor, T. P.: Novel Use of Time Domain Reflectometry in Infiltration-Based Low Impact Development Practices, J. Irrig. Drain. Eng., 139(8), 625–634, doi:10.1061/(ASCE)IR.1943-4774.0000595, 2013.

Timm, A., Kluge, B. and Wessolek, G.: Hydrological balance of paved surfaces in moist mid-latitude climate – A review, Landsc. Urban Plan., 175(April 2017), 80–91, doi:10.1016/j.landurbplan.2018.03.014, 2018.

Topp, G. C., Davis, J. L. and Annan, A. P.: Electromagnetic determination of soil water content: Measurements in coaxial transmission lines, Water Resour. Res., 16(3), 574–582, doi:10.1029/WR016i003p00574, 1980.

Trenberth, K. E. and Asrar, G. R.: Challenges and Opportunities in Water Cycle Research: WCRP Contributions, Surv. Geophys., 35(3), 515–532, doi:10.1007/s10712-012-9214-y, 2014.

Turco, M., Kodešová, R., Brunetti, G., Nikodem, A., Fér, M. and Piro, P.: Unsaturated hydraulic behaviour of a permeable pavement: Laboratory investigation and numerical analysis by using the HYDRUS-2D model, J. Hydrol., 554, 780–791, doi:10.1016/j.jhydrol.2017.10.005, 2017.

Vereecken, H., Huisman, J. A., Hendricks Franssen, H. J., Brüggemann, N., Bogena, H. R., Kollet, S., Javaux, M., Van Der Kruk, J. and Vanderborght, J.: Soil hydrology: Recent methodological advances, challenges, and perspectives, Water Resour. Res., 51(4), 2616–2633, doi:10.1002/2014WR016852, 2015.

Weiler, M. and Flühler, H.: Inferring flow types from dye patterns in macroporous soils, Geoderma, 120(1–2), 137–153, doi:10.1016/j.geoderma.2003.08.014, 2004.

Wessolek, G.: Sealing of soils, in Urban Ecology: An International Perspective on the Interaction Between Humans and Nature, pp. 161–179, Springer US, Boston, MA., 2008.

Winston, R. J., Al-Rubaei, A. M., Blecken, G. T., Viklander, M. and Hunt, W. F.: Maintenance measures for preservation and recovery of permeable pavement surface infiltration rate - The effects of street sweeping, vacuum cleaning, high pressure washing, and milling, J. Environ. Manage., 169, 132–144, doi:10.1016/j.jenvman.2015.12.026, 2016.

Zhu, K., Blum, P., Ferguson, G., Balke, K. D. and Bayer, P.: The geothermal potential of urban heat islands, Environ. Res. Lett., 5(4), doi:10.1088/1748-9326/5/4/044002, 2010.